[1] **Abdullah Marzouq Alharbi**

[2] **Azhar Abdul Rahman ***

[3] **Naser M. Ahmed**

[4] **Nurul Zahirah Noor Azman**

[5] **Mus'ab S Alkasasbeh**

Extended Gate Field-Effect Transistor Based on Quantum Dots Porous Silicon with Silver Nanowires for X-ray Dosimeter Applications

Abstract: - The development of a sensitive and reliable design of the extended gate field effect transistor (EGFET) for X-ray dosimeter is in demand for the measurement of radiation dose in several fields including diagnostic and interventional radiology. Here, porous silicon quantum dot (PSi-QD) was prepared from n-type silicon (100) using the photo–electrochemical etching technique and tested as an EGFET for X-ray detection. Well-defined crystalline silver nanowires (AgNWs) have been incorporated on the surface of bare PSi-QD through dropping a homogeneous AgNWs solution. The crystal structure and surface morphology of the prepared PSi-QD and AgNWs/PSi-QD were analyzed using X-ray diffraction (XRD) and field emission scanning electron microscopy (FESEM), respectively. The voltage sensitivity and linearity of both structures were then examined using low absorbed doses of 10, 39, and 59 mGy. The PSi-QD and AgNWs/PSi-QD EGFETs displayed voltage sensitivity and linearity values of 2.3 mV/mGy and 88.63%, and 3.0 mV/mGy and 94.44%, respectively. Furthermore, the measured sensitivity of the PSi-QD EGFET decreased from 2.9 mV/mGy to 2.2 mV/mGy, while that of AgNWs/PSi-QD EGFET reduced from 7.6 mV/mGy to 3.3 mV/mGy with increase in the absorbed dose from 10mGy to 59 mGy. Based on its high voltage sensitivity and good linearity as well as its good repeatability and measurable radiation sensitivity, the AgNWs/PSi-QD EGFET can be considered an effective and functional radiation dosimeter for X-ray detection.

Keywords: X-ray Dosimeter; PSi-QD; Silver nanowires; EGFET; Sensitivity.

I. INTRODUCTION

X-rays are a common source of ionizing radiation that can be exposed to in several fields such as health, industry and science. Thus, the proper radiation detection of these rays in these places is critical to protect the environment and the public from potential chronic diseases as a result of exposure to it. Accordingly, it is necessary to develop adequate radiation detection devices whose type is based on the energy range utilized [1]. Metal oxides are generally well known for their dosimetric application. Portable dosimeters derived from metal oxide semiconductor field effect transistors (MOSFETs) have several applications that include the monitoring of irradiation doses and instantly read radiation doses [2]. However, the insensitivity of MOSFETs to various conditions of the ambient environment, including light and temperature, has made the development of EGFET structure a critical task [1]. The design of EGFET entails connection of its sensing element to the end of a signal line, which is coupled to the gate of the MOSFET, and directly exposed to the irradiation. This allows the reuse of the EGFET structure several times without exposing the MOSFET to irradiation [3]. In this way, the commercial MOSFET is completely detached from the effects of its ambient conditions. Furthermore, larger samples might be employed with the EGSFET configuration devoid of the constraints posed by the size of the

[1] School of Physics, Universiti Sains Malaysia, Penang 11800, Malaysia

Physics Department, Collage of Science, Shaqra University, Shaqra 11961, Saudi Arabia. abdullahmarzouqalharbi@gmail.com

[2] School of Physics, Universiti Sains Malaysia, Penang 11800, Malaysia. arazhar@usm.my

[3] School of Physics, Universiti Sains Malaysia, Penang 11800, Malaysia

Department of Laser and optoelectronics engineering, Dijlah Universiti College, Baghdad, Iraq. nas_tiji@yahoo.com

[4] School of Physics, Universiti Sains Malaysia, Penang 11800, Malaysia.nzahirah@usm.my

[5] School of Physics, Universiti Sains Malaysia, Penang 11800, Malaysia. malkasasbeh@gmail.com

*Corresponding Author Email: arazhar@usm.my

MOSFET, which gives this design a broader detection area [4]. In addition, the EGFET is more compact, easy to handle, offers more accurate and rapid read out of radiation dosage, and exhibits low sensitivity to variations in external conditions in the course of conducting irradiation measurements.

Porous silicon (PSi) has been classified as one of the most promising source material for the production of EGFET [3, 5]. Over the years, PSi has been synthesized using various methods. One of such methods involves the chemical and electrochemical etching of crystalline Si in hydrofluoric acid (HF). Depending on the electrochemical conditions, parameters such as porosity (volumetric fraction of voids within Psi), thickness, and morphology (shape and pore size) can be modified, which allows the development of nano-sized crystallites on PSi [6]. Therefore, surface modification of the silicon wafer plays an important role in improving its sensitivity, which explains its successful use for an extensive array of radiation detection applications [7]. Furthermore, several applications of PSi have been investigated, such as light emitted diodes [8-10], photodetectors [11, 12], waveguides [13], and chemical sensors [14, 15]. PSi is also characterized by its relatively high surface to volume ratio with large effective sensing area [16], which has enabled its use as EGFET in a variety of radiation detection applications.

Recently, porous silicon quantum dots (PSi-QD) were developed in order to benefit from the intrinsic optoelectronic properties of PSi [17]. However, not much has been done on radiation detection and dosimetric applications of PSi-QD EGFET. Thus, a breakthrough is necessary in this field in order to achieve active extended gates with high detection sensitivity. To improve their radiation detectability, the electronic and structural properties of PSi-QDs have been enhanced through the appropriate selection of different metallic elements such as Ga, Al, Cu, Ag, Au, and Pt to serve as the detection layer [18, 19]. Among of these elements, Ag nanowires (AgNWs) is proven to be appropriate for doping PSi-QD structures because of its outstanding optical and electrical properties, which strongly depend on size, shape and composition [20]. In addition, AgNWs display excellent physicochemical properties such as huge effective scattering cross section and surface plasmon resonance (SPR) [21]. Therefore, PSi-QD doped with AgNWs is expected to be an effective candidate for the fabrication of active extended gates for radiation detection and dosimetric uses.

Accordingly, this study employed the photo-electrochemical etching technique to prepare PSi-QD from n-type Si wafer with (100) orientation. Afterwards, the surface of the PSi-QD structure was modified by doping with AgNWs via a simple and well-controlled method. The crystallinity and morphology of the PSi-QD and AgNWs doped PSi-QD samples were investigated. The potential use of the prepared samples as EGFET, i.e. X-ray radiation detector was then studied. The performance and sensitivity of the samples under various X-ray doses were analyzed.

II. Materials And Methods

2.1 Fabrication and characterization of Psi-QD with AgNWs

Photo-electrochemical etching process was utilized to fabricate the PSi-QD samples. An n-type single side polished Si (100) wafer with resistivity and thickness of 5–10 Ω cm and 256–306 μm, respectively, was used in the etching process. The diamond cutter was used to cut the Si wafer into rectangle pieces with a dimension of (1.0 cm × 1.5 cm) to serve as an anode in the electrochemical etching cell against the cathode of tungsten wire. The Si wafer was then cleaned in line with the standard procedure by the Radio Corporation of America (RCA) to eliminate the possibility of contamination during cutting process. After the cleaning process, the Si wafer was etched in a Teflon cell holding a solution of hydrofluoric acid (HF; 47% purity) and ethanol (C_2H_5OH 99%) mixed at a volume ratio of 1:1. All the chemical materials were procured from Sigma-Aldrich. The Si wafer was subsequently etched using a DC current under room temperature at a current density of 40 mA/cm^2 for 20 min. A tungsten lamp was used as the external light source to illuminate the cell. After that, the solution was disposed, and the sample was rinsed with ethanol and de-ionized water multiple times to avoid the growth of the native oxide SiO_2 layer, and then dried under nitrogen gas flow. The photo-electrochemical etching procedure is illustrated in Fig. 1(a).

Following the etching procedure, well-defined crystalline AgNWs were incorporated on the bare PSi-QD via a simple and well-controlled method. Homogeneous AgNWs solution was dropped on the bare PSi-QD that is placed on a hot-plate set to 80 °C. The sample was left on the hotplate for 5 mins, and then cooled down to room

temperature. The morphology and crystallinity of PSi-QD with and without AgNWs were investigated. Field emission scanning electron microscopy (FESEM, FEI Nova nano SEM 450) coupled with energy dispersive X-ray (EDX) part was used to characterize the morphology and elemental composition of the samples. The structure of the bare PSi-QD, as well as with AgNWs, was examined using a high-resolution X-ray diffractometer (XRD) (X'pert PRO, Philips, Eindhoven, Netherlands) and the spectra were collected between 2θ of (20 and 80)° at a step width of 0.02°. Uv-visible absorption spectroscopy (Hitachi-330 spectrophotometer) was utilized to record the absorption spectrum of the AgNWs from the aqueous suspension in the range of 300-700 nm.

2.2 Fabrication of EGFET and sensitivity measurements

Silver electrodes were deposited onto the outer area of the prepared samples to make an Ohmic contact through a metal mask with a fingerprint interdigitated shape using the DC/RF sputtering technique. Conductive wires were then connected to the synthesized fingerprint interdigitated electrodes using silver paste. Afterwards, the samples were attached to a commercialized MOSFET (CD4007UB) as an extended gate to keep it away during irradiation exposure. The current–voltage (I-V) characteristics curves were then measured under a low absorbed dose of X-ray radiation starting from 0, 10, 31 and 59 mGy using the X-ray machine at the School of Physics, USM, Penang, Malaysia. The I-V characteristics were recorded using two Keithley 2400 source measure units (SMUs) connected to a personal computer and LabTracer 2 software was utilized to initiate the measurements and record the data. All measurements were performed at room temperature. The measurement setup in this work is shown in Fig. 1(b).The configuration shown in the figure and used in this study is mentioned in [22]. The PSi-QD electrode was connected to a gate terminal of the commercial MOSFET. Before attaching the PSi-QD electrode to the measuring equipment, it was exposed to an X-ray source.

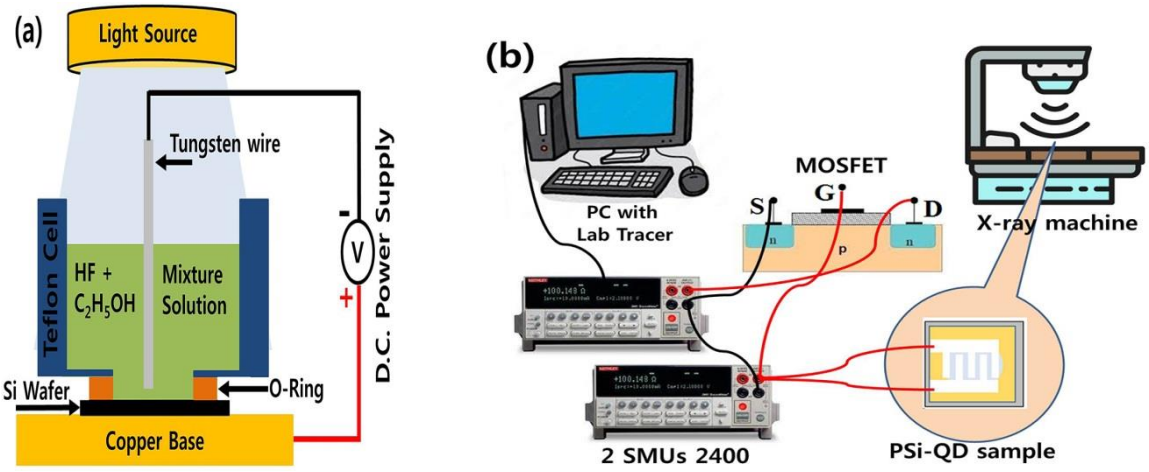

Figure -1 (a) A schematic diagram of the photo-electrochemical method used for the preparation of PSi-QD sample. (b) A schematic of the measurement setup in this work.

III. Results And Discussion

Prior to using the both samples as extended gates with the MOSFET structure, the crystalline nature was initially examined by XRD analysis. The collected XRD pattern for PSi-QD and AgNWs/PSi-QD samples are illustrated in Fig. 2 (a and b). As shown in Fig. 2a, the PSi-QD sample showed only one diffraction peak observed at 2θ of about 69.14° which is assigned to the (001) plan of Si according to the standards (JCPDS) [23]. On the other hand, AgNWs/PSi-QD sample showed two diffraction peaks at 2θ angles of about 38.11°, and 44.34° (Fig. 2b), which matches the (111), and (002) planes of a face-centered cubic crystal of silver, respectively, according to the standard JCPDS card number 01-089-3722 [24]. The presence of the sharp peak located at 2θ =38.11° clearly confirms the high crystalline quality of the sample, which is further supported by the FE-SEM results. The crystallite size for AgNWs/PSi-QD was calculated from the diffraction peak with the highest intensity, using the Scherer's formula [25], refer to Eq. (1):

$$D = K\lambda/\beta Cos\theta \quad (1)$$

where K= 0.9, λ = 0.15418 nm, β and θ represent shape factor, X-ray wavelength, corrected line broadening at half maximum in radians, and Bragg's angle, respectively. The calculated crystallite size was about 57 nm.

Another factor that determines the quality of nanostructure materials is the specific surface area (SSA). The SSA was also evaluated from the most intense XRD peak using the following equation (Eq. (2)) [26], which was 10.03 m^2/gm:

$$SSA = 6000/D\rho \quad (2)$$

where, ρ is the density of the silver (10.49) g/cm^3. The high SSA of AgNWs/PSi-QD made it a promising candidate for radiation sensor with high detection sensitivity.

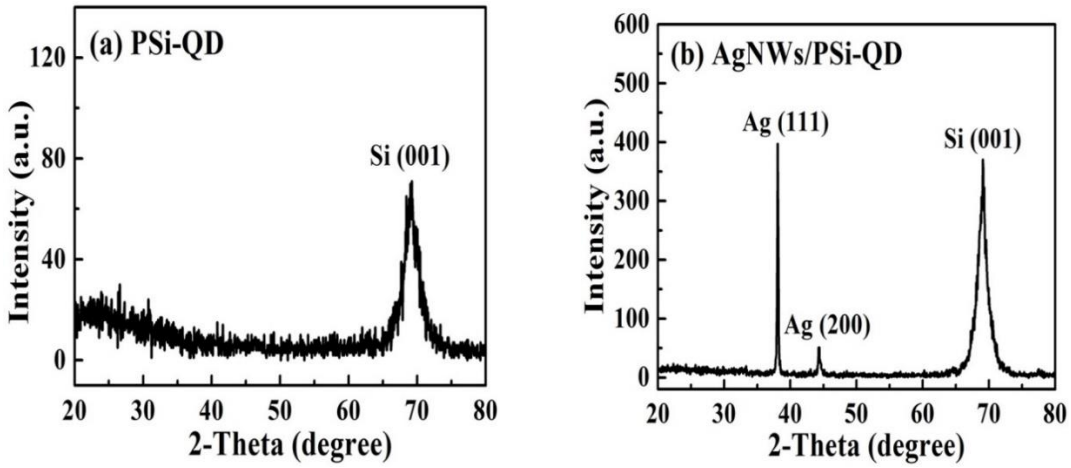

Figure -2 XRD patterns of a prepared (a) PSi-QD sample and (b) AgNWs/PSi-QD sample.

The surface microtexture and elemental composition of PSi-QD and AgNWs/PSi-QD samples were examined using FE-SEM and EDX analysis, as shown in Fig. 3. Figure 3(a). The top view of the PSi-QD sample shows almost spherical and irregularly shaped porous nanostructures that are densely and randomly distributed on the surface. Because of the presence of QD size pores on the surface, the AgNWs can form on the interfaces between the QD pores. At the same time, the pores are not blocked by the nanowires, which increase the effective surface area of the sample. Figure 3(b) presents a micrograph image of AgNWs, which shows the presence of a large concentration of AgNWs with various lengths and diameters in the ranges of several micrometers and tens of nanometers, respectively. The corresponding aspect ratio of these nanowires is determined to be very high. Therefore, the very small size of the pores in the PSi-QD layer prevents the AgNWs entering inside them; thus they aggregate on the surface of the PSi-QD. The statistical distribution of the nanowires diameter is determined by the Image J software program and is presented in the inset of Fig. 3(b). It shows that the diameter of AgNWs ranges from 18 nm to 92 nm, and the peak of the AgNWs diameter distribution is about 28 nm.

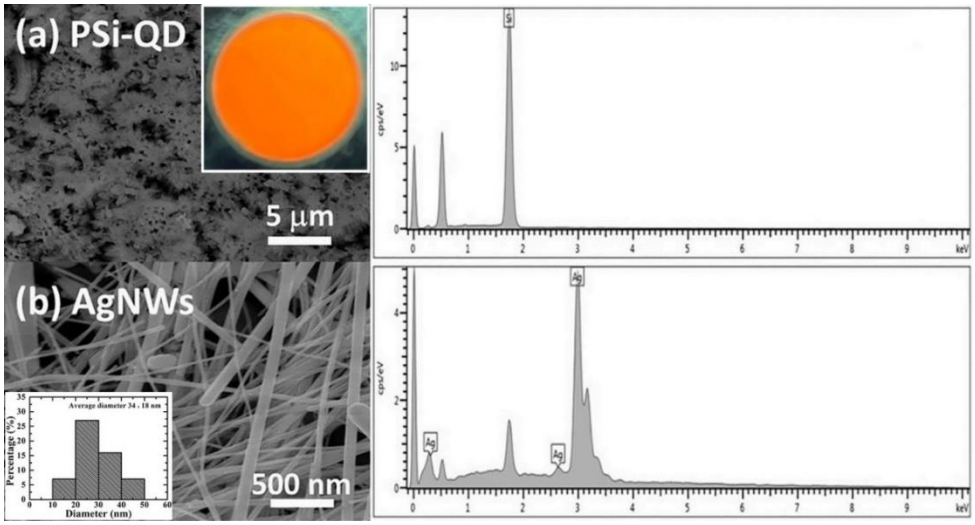

Figure -3 FE-SEM images and their EDX of (a) PSi-QD sample. Inset shows the optical image of the PSi-QD surface. (b) AgNWs/PSi-QD sample. Inset shows the statistical distribution of AgNWs diameter.

The UV–visible absorption spectrum for the aqueous suspension of AgNWs is shown in Fig. 4. The peak positioned around 400 nm is mainly due to the transverse plasmon excitation of AgNWs. The plasmon response of bulk silver caused the shoulder peak observed around 352 nm, which is commonly characteristic of AgNWs [27].

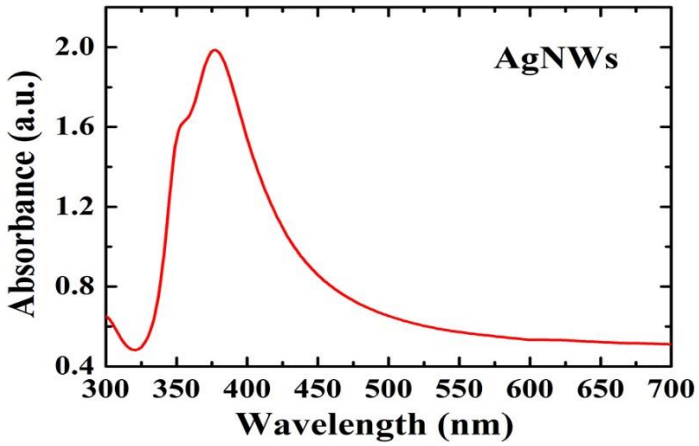

Figure -4 UV-visible absorption spectra of AgNWs

The technique shown in Fig. 1(b) was utilized to record the (I_{ds}-V_{gs}) and (I_{ds}-V_{ds}) characteristics curves for linear and saturation regimes, respectively. The I-V curves for the prepared PSi-QD and AgNWs/PSi-QD EGFETs with various X-ray doses of 0, 10, 31, and 59 mGy for both linear and saturation regimes are shown in Figs. 5 (a-d), respectively. A fixed V_{ds} (drain-to-source voltage) value of 0.2 V was applied for the linear regime, while a gate-to-source voltage (V_{gs}) was maintained at 2 V for the saturation regime. As shown in Fig. 5, in the linear regime curves, the threshold voltage was shifted to the lower values as the absorbed dose was increased. On the other hand, in the saturation regime curves, the current recorded higher values as the X-ray radiation dose was increased to 59 mGy. In the saturation regime, the increase in current levels could be mainly attributed to the formation of electron–hole pairs as the electrical properties were improved during irradiation [25]. The interaction of X-rays with a material is basically anchored in excitation and ionization of electrons, and atomic migration of outer electrons [26].The current level increment for PSi-QD and AgNWs/PSi-QD EGFETs was about 11.3 µA and 17.1 µA under the same absorbed dose of 59mGy, respectively.

The voltage sensitivity and linearity values of the PSi-QD and AgNWs/PSi-QD EGFETs were derived from the linear regime by plotting a linear curve between V_{gs} and dose value at a fixed I_{ds} of 0.4 mA, as shown in Fig. 6 (a and b). The linearity of the curve was obtained from Origin Pro software and the sensitivity was measured from the slope of the fitting line. As observed in the figure, the voltage response of the system decreased with increase in the absorbed dose up to 59 mGy for both devices, within standard error of <5%, which indicates very good repeatability. The voltage sensitivity from the linear regime was estimated to be 2.3 mV/mGy with a linearity of 88.63% for the PSi-QD EGFET and 3.0 mV/mGy with a linearity of 94.44% for the AgNWs/PSi-QD EGFET. The results show a strong linear dependence of the voltage response on the dose values in the linear region. The higher sensitivity with excellent linearity of the fabricated AgNWs/PSi-QD device is attributed to the large sensing area of AgNWs and high PSi-QD absorption properties.

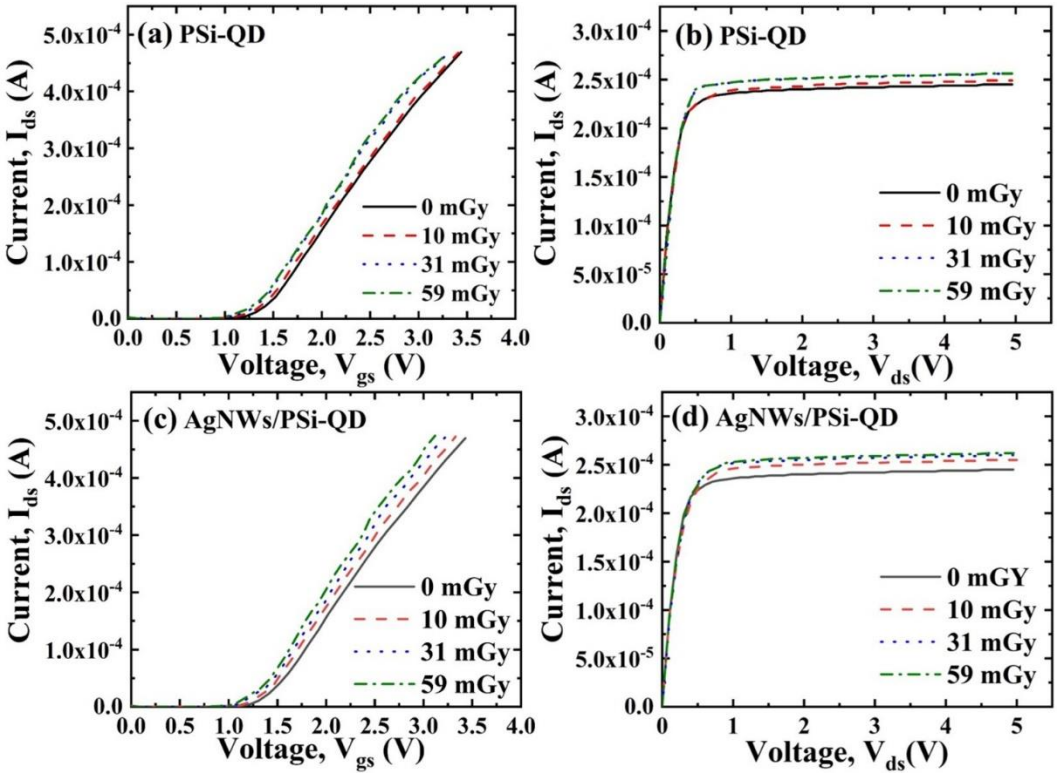

Figure -5 I_{ds}-V_{gs} and I_{ds}-V_{ds} characteristics for the prepared (a and b) PSi-QD EGFET and (c and d) AgNWs/PSi-QD EGFET in the linear and saturation regimes, respectively.

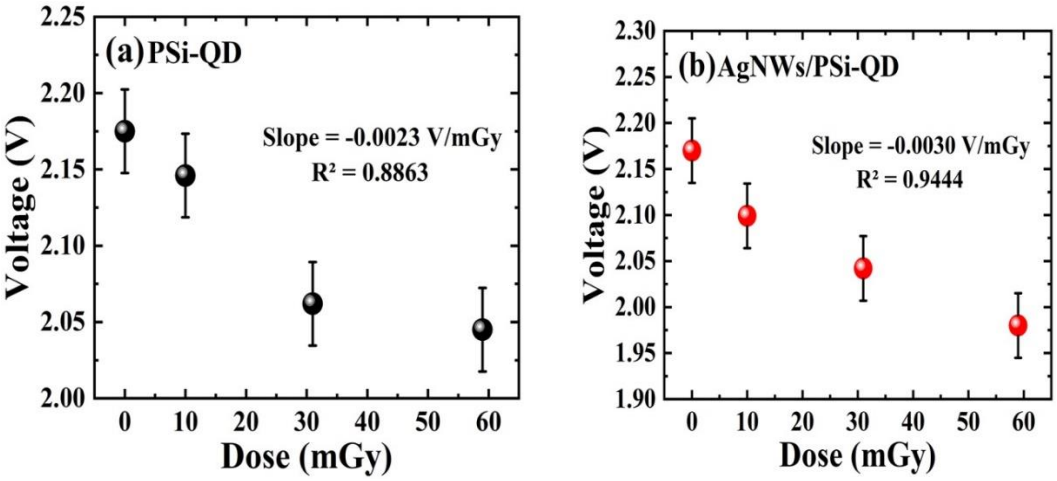

Figure -6 Voltage sensitivity and linearity as a function X-ray dose values of the prepared (a) PSi-QD and (b) AgNWs/PSi-QD EGFETs.

The threshold voltage (V_{TH}), the intersection of linear component of the curve with the V_{gs} axis in the linear regime, was calculated using the underlying Eq. (3) for both devices [19]:

$$\Delta V_{TH} = V_{TH} - V_{THo} \quad (3)$$

Where V_{THo} and V_{TH} are the values of the threshold voltages pre- and post exposure to irradiation, respectively. The estimated values of threshold voltage for the both devices at the different exposure doses are plotted in Fig. 7(a) and presented in Table 1. According to the figure, the ΔV_{TH} increased for all samples with increase in the absorbed dose value. The detection sensitivity (S) of the PSi-QD and AgNWs/PSi-QD extended gates to X-ray exposure was calculated in terms of ΔV_{TH} according to Eq. (4) [19]:

$$S = \Delta V_{TH}/D \quad (4)$$

where D is the absorbed dose value. The calculated values of the sensitivity as a function of the absorbed dose are plotted in Fig. 7(b) and listed in Table 1. As the absorbed doses increases, the sensitivity of the both dosimeters

decreased. However, the sensitivity improved from 2.2 mV/mGy for the PSi-QD dosimeter to 3.3 mV/mGy for the AgNWs/PSi-QD dosimeter under the same radiation dose of 59 mGy. These results were much higher than that recorded from the ZnO-Pb thin film (1.42 mV/mGy) under X-ray radiation dose of 70 mGy [1]. Furthermore, the obtained sensitivity of the PSi-QD EGFET at the lowest absorbed dose of 10 mGy was 2.9 mV/mGy, while the sensitivity of the AgNWs/PSi-QD EGFET was 7.6 mV/mGy at the same absorbed dose, which is also higher than that mentioned previously in [1]; it was about 6.42 mV/mGy at absorbed dose of 9 mGy. Based on the results mentioned above, the noticeable improvement in the radiation detection sensitivity of these devices can be attributed to changes in the effective electric field manifested by the EGFET during irradiation, resulting in a accretion of holes at the gate oxide contact [27]. The AgNWs/PSi-QD EGFET based X-ray dosimeter can be considered viable for real-time-radiation dosimetry at room temperature based on its high voltage sensitivity, good linearity, good repeatability and radiation sensitivity.

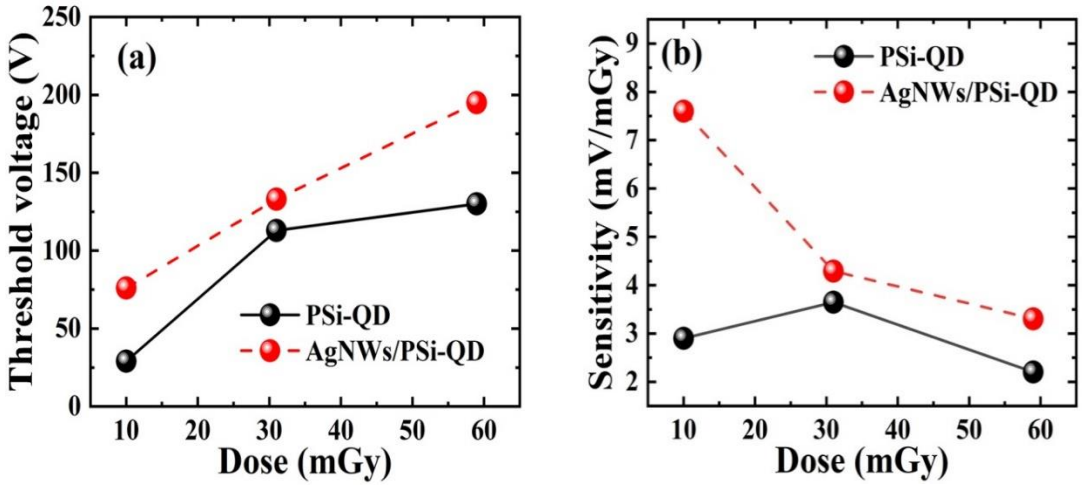

Figure -7. (a) Threshold voltage vs. X-ray dose and (b) sensitivity vs. X-ray dose for both the prepared PSi-QD and AgNWs/Psi-QD EGFETs.

Table 1- Radiation sensing characteristics for both the prepared PSi-QDand AgNWs/Psi-QD EGFET

EGFET	X-ray absorbed dose (mGy)	Threshold Voltage (mV)	Sensitivity (mV/mGy)	Linearity (%)
PSi-QD	10	29	2.9	88.63
	31	113	3.6	
	59	130	2.2	
AgNWs/PSi-QD	10	76	7.6	94.44
	31	133	4.3	
	59	195	3.3	

IV. CONCLUSION

In summary, PSi-QD was prepared in this study using the photo-electrochemical etching technique, after which AgNWs was successfully incorporated on its surface to be used as an EGFET for X-ray dosemeter. The crystallinity and nanometric size of the synthesized AgNWs/PSi-QD were determined using XRD and FESEM measurements. The sensing property of PSi-QD and AgNWs/PSi-QD extended gates was examined using low absorbed doses of 10, 39, and 59 mGy. The I-V characteristics in linear and saturation regimes of the both EGFETs were recorded to estimate the changes in the threshold voltage and to measure the radiation sensitivity. The threshold voltage for both structures was shifted to left by increasing the absorbed dose. In addition, the AgNWs/PSi-QD sensor demonstrated the highest value of sensitivity of 7.6 mV/mGy at the lowest absorbed dose value of 10 mGy.

ACKNOWLEDGEMENT

The authors would like to thank the School of Physics at USM University for providing the research facilities and support. We appreciate the financial support from the RCMO USM through the Short-Term Grant (304/PFIZIK/6315514).

CONFLICT OF INTEREST

The authors declare that they have no conflicts of interest.

REFERENCES

[1] A. M. Ahmed Ali, N. M. Ahmed, N. A. Kabir, M. K. M. Ali, H. Akhdar, O. A. Aldaghri, *et al.*, "Investigation of X-ray Radiation Detectability Using Fabricated ZnO-PB Based Extended Gate Field-Effect Transistor as X-ray Dosimeters," *Applied Sciences*, vol. 11, p. 11258, 2021.

[2] I. Thomson, R. Thomas, and L. Berndt, "Radiation dosimetry with MOS sensors," *Radiation Protection Dosimetry*, vol. 6, pp. 121-124, 1983.

[3] N. M. Ahmed, E. Kabaa, M. Jaafar, and A. Omar, "Characteristics of extended-gate field-effect transistor (EGFET) based on porous n-type (111) silicon for use in pH sensors," *Journal of electronic Materials*, vol. 46, pp. 5804-5813, 2017.

[4] N. H. Al-Hardan, M. A. Abdul Hamid, N. M. Ahmed, A. Jalar, R. Shamsudin, N. K. Othman, *et al.*, "High sensitivity pH sensor based on porous silicon (PSi) extended gate field-effect transistor," *Sensors*, vol. 16, p. 839, 2016.

[5] H. A. Santos, "Porous silicon for biomedical applications," 2014.

[6] W. Z. Tawfik, G. Y. Hyun, S.-W. Ryu, J. S. Ha, and J. K. Lee, "Piezoelectric field in highly stressed GaN-based LED on Si (1 1 1) substrate," *Optical Materials*, vol. 55, pp. 17-21, 2016.

[7] P. Fauchet, J. Von Behren, K. Hirschman, L. Tsybeskov, and S. Duttagupta, "Porous silicon physics and device applications: a status report," *physica status solidi (a)*, vol. 165, pp. 3-13, 1998.

[8] L. Canham, T. Cox, A. Loni, and A. Simons, "Progress towards silicon optoelectronics using porous silicon technology," *Applied surface science*, vol. 102, pp. 436-441, 1996.

[9] B. Ünal, A. Parbukov, and S. Bayliss, "Photovoltaic properties of a novel stain etched porous silicon and its application in photosensitive devices," *Optical Materials*, vol. 17, pp. 79-82, 2001.

[10] L. Balagurov, S. Bayliss, D. Yarkin, S. Y. Andrushin, V. Kasatochkin, A. Orlov, *et al.*, "Low noise photosensitive device structures based on porous silicon," *Solid-State Electronics*, vol. 47, pp. 65-69, 2003.

[11] T. Hadjersi and N. Gabouze, "Photodetectors based on porous silicon produced by Ag-assisted electroless etching," *Optical Materials*, vol. 30, pp. 865-869, 2008.

[12] C. Liyanage and D. Blackwood, "Functionalization of a porous silicon impedance sensor," *Thin Solid Films*, vol. 550, pp. 677-682, 2014.

[13] E. Massera, I. Nasti, L. Quercia, I. Rea, and G. Di Francia, "Improvement of stability and recovery time in porous-silicon-based NO2 sensor," *Sensors and Actuators B: Chemical*, vol. 102, pp. 195-197, 2004.

[14] J. Kanungo, H. Saha, and S. Basu, "Room temperature metal–insulator–semiconductor (MIS) hydrogen sensors based on chemically surface modified porous silicon," *Sensors and Actuators B: Chemical*, vol. 140, pp. 65-72, 2009.

[15] S. Hosseini, I. A. Sarsari, P. Kameli, and H. Salamati, "Effect of Ag doping on structural, optical, and photocatalytic properties of ZnO nanoparticles," *Journal of Alloys and Compounds*, vol. 640, pp. 408-415, 2015.

[16] M. Mori, P. V. Almeida, M. Cola, G. Anselmi, E. Mäkilä, A. Correia, *et al.*, "In vitro assessment of biopolymer-modified porous silicon microparticles for wound healing applications," *European Journal of Pharmaceutics and Biopharmaceutics*, vol. 88, pp. 635-642, 2014.

[17] D. Kumar, Kavita, K. Singh, V. Verma, and H. Bhatti, "Microwave-assisted synthesis and characterization of silver nanowires by polyol process," *Applied Nanoscience*, vol. 5, pp. 881-890, 2015.

[18] Y.-e. Shi, L. Li, M. Yang, X. Jiang, Q. Zhao, and J. Zhan, "A disordered silver nanowires membrane for extraction and surface-enhanced Raman spectroscopy detection," *Analyst*, vol. 139, pp. 2525-2530, 2014.

[19] A. M. A. Ali, N. M. Ahmed, N. A. Kabir, and M. A. Almessiere, "Multilayer ZnO/Pb/G thin film based extended gate field effect transistor for low dose gamma irradiation detection," *Nuclear Instruments and Methods in Physics Research Section A: Accelerators, Spectrometers, Detectors and Associated Equipment*, vol. 987, p. 164833, 2021.

[20] I. Kokal, O. Göbel, E. Van den Ham, J. E. ten Elshof, P. Notten, and H. Hintzen, "Patterning of lithium lanthanum titanium oxide films by soft lithography as electrolyte for all-solid-state Li-ion batteries," *Ceramics international*, vol. 41, pp. 13147-13152, 2015.

[21] Z. Cheng, L. Liu, S. Xu, M. Lu, and X. Wang, "Temperature dependence of electrical and thermal conduction in single silver nanowire," *Scientific reports*, vol. 5, p. 10718, 2015.

[22] M. M. Ahmed, W. Z. Tawfik, M. Elfayoumi, M. Abdel-Hafiez, and S. El-Dek, "Tailoring the optical and physical properties of La doped ZnO nanostructured thin films," *Journal of Alloys and Compounds*, vol. 791, pp. 586-592, 2019.

[23] A. M. Alwan, A. A. Yousif, and L. A. Wali, "The growth of the silver nanoparticles on the mesoporous silicon and macroporous silicon: a comparative study," 2017.
[24] K. E. Korte, S. E. Skrabalak, and Y. Xia, "Rapid synthesis of silver nanowires through a CuCl-or CuCl 2-mediated polyol process," *Journal of Materials Chemistry*, vol. 18, pp. 437-441, 2008.
[25] K. Arshak, J. Corcoran, and O. Korostynska, "Gamma radiation sensing properties of TiO2, ZnO, CuO and CdO thick film pn-junctions," *Sensors and Actuators A: Physical*, vol. 123, pp. 194-198, 2005.
[26] R. El-Mallawany, A. Abousehly, A. El-Rahamani, and E. Yousef, "Radiation effect on the ultrasonic attenuation and internal friction of tellurite glasses," *Materials chemistry and physics*, vol. 52, pp. 161-165, 1998.
[27] M. C. Lavallée, L. Gingras, and L. Beaulieu, "Energy and integrated dose dependence of MOSFET dosimeter sensitivity for irradiation energies between and," *Medical physics*, vol. 33, pp. 3683-3689, 2006.